Journal of Zhejiang University-SCIENCE C (Computers & Electronics)
ISSN 1869-1951 (Print); ISSN 1869-196X (Online)
www.zju.edu.cn/jzus; www.springerlink.com
E-mail: jzus@zju.edu.cn

Comparison of resonant current regulators for DFIG during grid voltage distortion*

Yi-peng SONG, Heng NIAN†‡

(*College of Electrical Engineering, Zhejiang University, Hangzhou 310027, China*)

†E-mail: nianheng@zju.edu.cn

Received May 12, 2013; Revision accepted Sept. 20, 2013; Crosschecked Nov. 18, 2013

Abstract: We investigate two different kinds of resonant current regulators for a doubly fed induction generator (DFIG) under distorted grid voltage conditions: proportional integral resonant (PIR) regulator with traditional resonant part and vector proportional integral (VPI) regulator with VPI resonant part. Based on the mathematical model of DFIG under distorted grid voltage, the transfer function and frequency response characteristics of the two current regulators are analyzed and compared. The superiority of the VPI current regulator over the PIR regulator is pointed out, and the influence of discretization methods on the performance of the resonant current regulator is studied. All the results are validated by MATLAB simulation and experiments.

Key words: Doubly fed induction generator, Harmonically distorted grid voltage, Resonant current regulator, Vector PI current regulator, Discretization method

doi:10.1631/jzus.C1300125 **Document code:** A **CLC number:** TM31

1 Introduction

Wind power generation based on a doubly fed induction generator (DFIG) has been increasingly popular due to its smaller converter rating around 25%–30% of the generator rating, variable speed operation, and four-quadrant active and reactive power control capabilities (Muller *et al.*, 2002; Iwanski and Koczara, 2008). To implement the stable operation and maximum power point track for DFIG, several new control strategies have been reported, including direct virtual torque control (Arbi *et al.*, 2009), predictive current control (Xu *et al.*, 2009), and control with an indirect matrix converter (Pena *et al.*, 2011).

Up to now, the steady-state and transient response of the DFIG-based wind power generation system under balanced (Luna *et al.*, 2011) and unbalanced (Xu and Wang, 2007; Hu and He, 2009; Hu *et al.*, 2009; 2010) grid voltage conditions have been investigated widely. In a practical situation, however, both transmission and distribution networks would contain voltage harmonic distortions. If the voltage harmonics in the power supply are not taken into account in DFIG's control strategy, highly distorted stator and rotor currents and significant torque and power oscillations would occur (Singh, 2009).

DFIG system operation under distorted grid voltage conditions was initially studied by Ramos *et al.* (2007). By adding a harmonic control scheme to the rotor current controller, the steady-state harmonic components in the stator currents were eliminated. Hu *et al.* (2011) presented an analysis and improved control of a wind turbine driven DFIG in which the alternative control targets were proposed to keep the three-phase stator currents or rotor currents sinusoidal, or remove pulsations in both stator active and reactive powers or in the generator's electromagnetic torque and stator reactive power. Liu *et al.* (2012; 2013) proposed a proper proportional integral resonant (PIR) regulator to eliminate the DFIG stator current

‡ Corresponding author

* Project supported by the National High-Tech R&D Program (863) of China (No. 2011AA050204) and the National Natural Science Foundation of China (No. 51277159)

harmonic component under distorted grid voltage and DC-voltage fluctuation under unbalanced grid voltage. Nian and Song (2014) proposed a direct power control (DPC) strategy for DFIG under grid voltage distortion with the vector proportional integral (VPI) controller. Nevertheless, it is quite common to apply the PIR regulator (Fukuda and Imamura, 2005; Etxeberria-Otadui *et al.*, 2006; Lascu *et al.*, 2007; 2009) to improve DFIG operation performance under distorted grid voltage conditions. However, the comparison of PIR controllers and VPI controllers when applied in DFIG control under the harmonic grid condition has not been investigated or analyzed.

To obtain an accurate tracking of rotor harmonic current reference, a traditional PI current regulator can be used to deal with each harmonic sequence in its respective rotating reference frame. Note that the decomposition of harmonic components and reference frame rotation is indispensable, which will deteriorate the system dynamic response due to the time delay and errors. The PIR current regulator could also achieve a zero steady state control error for the rotor current in the synchronous reference frame, with the PI part dealing with the fundamental component and the resonant part dealing with the harmonic components. However, the harmonic current tracking capability of the resonant part in PIR would be limited due to the phase shift of the closed-loop phase-frequency response at the resonant frequency, which will degrade rotor current signal tracking precision.

The VPI current regulator (Lascu *et al.*, 2007; 2009), which is based on pole-zero cancellation to enhance the harmonic current control ability, was introduced to replace the PIR regulator. It was reported in Lascu *et al.* (2007; 2009) that compared with the PIR regulator, the VPI regulator has superior performance in terms of stability and bandwidth and can maintain stable operation at high frequencies, which is helpful for control of the DFIG harmonic current. Furthermore, it will be explicitly illustrated in this paper that the inherent 90° leading phase response at the resonant frequency of the VPI current regulator would make it much more appropriate to control DFIG which is always considered as an inertia load.

In practical situations, when grid frequency may deviate slightly from the rated fundamental frequency, the implementation of resonant frequency bandwidth ω_c in VPI or PIR would be helpful in improving the DFIG harmonic control performance by reducing the sensitivity of the resonant regulator to grid frequency variation (Hu and He, 2009; Hu *et al.*, 2009; 2010; 2011; Liu *et al.*, 2012; 2013; Nian and Song, 2014). Nevertheless, note that according to Zmood and Holmes (2003), the resonant frequency bandwidth ω_c (which is called the damping factor in Zmood and Holmes (2003)) is not preferred since the gain of the resonant controllers in the vicinity of the resonant peak is lower as ω_c gets higher. Therefore, Zmood and Holmes (2003) concluded that if a damping factor must be used, it should be implemented with as small a value as possible.

Note that most literature about resonant regulators was devoted to certain grid-tied interfacing converters, such as the active power filter (APF) (Bojoi *et al.*, 2005; Fukuda and Imamura, 2005; Lascu *et al.*, 2007; 2009; Li *et al.*, 2010; Yepes *et al.*, 2010), in which the harmonic current caused by non-linear load can be compensated with the highest order of harmonic current component typically around the 40th order. However, when the resonant regulator is applied for DFIG control, the stator winding is directly connected to the power grid, which is considered as the harmonic source and contains mainly low order grid voltage harmonics composed of the 5th and 7th sequence components. Grid voltage harmonic components higher than 7th order may be tiny enough to be neglected (IEEE Standard 519-1992; Gambica, 2005). Thus, it is reasonable to investigate the control capability of the resonant regulator in terms of regulation of 5th and 7th order harmonic components in DFIG applications, which will be the main concern of this study.

As the transfer functions of PIR and VPI current regulators are normally designed in the continuous domain, it is quite important to employ an appropriate discretization method to ensure that the discrete form of current regulator can exactly match the continuous one. An inappropriate discretization method would cause the zeros and poles shift of the transfer function, which will deteriorate the regulator stability and reduce the tracking precision (Yepes *et al.*, 2010).

The phase delay effect of the resonant regulator is also a key factor for accurate control of the harmonic frequency. Yuan *et al.* (2002) proposed a phase leading technique for the PIR regulator to compensate both the phase delay response of PIR closed-loop

control and the system delay of one control period, in which an accurate phase delay calculation based on the control subject parameters and AD sample frequency is required. Thus, the delay compensation technique for the PIR regulator would be inapplicable in practical situations with the variable control subject parameters. However, the phase delay response of closed-loop control using the VPI regulator can be avoided, which will be investigated in Section 2.2. Therefore, only the system delay in the control loop based on the VPI regulator needs to be compensated, so it is convenient for VPI implementation in practical situations.

This paper investigates and compares the PIR and VPI current regulators used to improve the operation performance of wind turbine driven DFIG generation systems under distorted grid voltage conditions. To compare the current tracking capability of the PIR and VPI regulators, sinusoidal stator current is chosen as the harmonic control target. First, the transfer function and frequency response of closed-loop control using both PIR and VPI regulators are analyzed and compared. Then, a discretization method for PIR and VPI regulator transfer function is discussed in the continuous domain. Finally, the comparison between PIR and VPI regulators is validated by both theoretical analysis and experiments conducted on a 1 kW laboratory set up DFIG system.

2 Comparison of PIR and VPI current regulators

Considering that the main objective of this paper is to implement accurate tracking of the rotor harmonic current, the mechanic component of the DFIG system, for instance, the wind turbine, bearing, and gear-box, will be ignored in the following discussion. To achieve the harmonic control target of keeping the sinusoidal three-phase stator currents, the tracking precision and control stability of the PIR and VPI current regulators will be investigated and compared.

Fig. 1 shows the T-representation of the DFIG equivalent circuit in the positive synchronous $(dq)^+$ reference frame rotating at the synchronous speed of ω_1.

The DFIG transfer function in a synchronous frame (Hu *et al.*, 2011) can be applied to analyze the

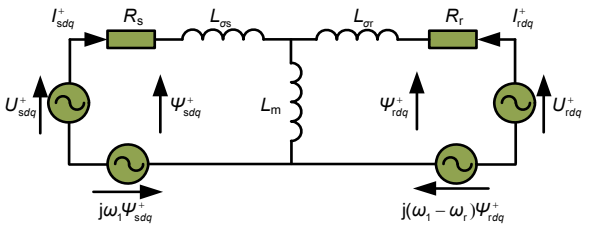

Fig. 1 T-representation of the DFIG equivalent circuit in the positive synchronous $(dq)^+$ reference frame rotating at the speed of ω_1

open- and closed-loop rotor harmonic current tracking capability:

$$G_p(s)=\frac{I_{rdq}(s)}{U_{rdq}(s)}=\frac{1}{s\sigma L_r+R_r}, \tag{1}$$

where I is the current, U is the voltage, subscript rdq is the rotor dq-axis component, L_r is total inductances of rotor winding, R_r is the rotor resistance, $\sigma=1-L_m^2/(L_sL_r)$ is the leakage factor, L_m is the mutual inductance, L_s is the stator inductance, and L_r is the rotor inductance.

Hu *et al.* (2011) also gave the rotor current reference in a synchronous frame with both the fundamental and harmonic components presented as

$$\begin{aligned} I_{rd}^{+*}&=I_{rd+}^{+*}+I_{rd5-}^{+*}+I_{rd7+}^{+*}\\ &=\frac{2P_s^*L_s}{3U_{sd+}^+L_m}-\frac{U_{sq5-}^{5-}}{5\omega_1L_m}e^{-j6\theta_s}+\frac{U_{sq7+}^{7+}}{7\omega_1L_m}e^{j6\theta_s}, \end{aligned} \tag{2a}$$

$$\begin{aligned} I_{rq}^{+*}&=I_{rq+}^{+*}+I_{rq5-}^{+*}+I_{rq7+}^{+*}\\ &=-\frac{2Q_s^*L_s}{3U_{sd+}^+L_m}-\frac{U_{sd+}^+}{\omega_1L_m}+\frac{U_{sd5-}^{5-}}{5\omega_1L_m}e^{-j6\theta_s}-\frac{U_{sd7+}^{7+}}{7\omega_1L_m}e^{j6\theta_s}. \end{aligned} \tag{2b}$$

Herein P and Q are stator active and reactive power; ω_1 is the angular speed of the grid voltage fundamental component; subscript sdq denotes the stator dq-axis component, subscripts +, 5−, 7+ represent the fundamental, 5th order harmonic, and 7th order harmonic components, respectively; superscripts +, 5−, and 7+ represent the synchronous, 5th order harmonic, and 7th order harmonic reference frames rotating at the angular speeds of +100π, −500π, and +700π rad/s, respectively; superscript * denotes the reference signal; θ_s is the phase angle of the grid

voltage fundamental component.

As can be seen from Eq. (2), the rotor current reference in a synchronous frame contains a DC component, as well as an AC component pulsating at six times grid voltage frequency, which will be regulated by the PI part and resonant part of PIR and VPI regulators, respectively. The DFIG parameters in the following discussion can be found in Table 3.

2.1 Transfer functions of PIR and VPI

Considering that slight frequency variation is always inevitable in the practical grid, a small resonant frequency bandwidth ω_c is applied in VPI and PIR regulator analysis in the following discussion, to enhance the harmonic control capability of DFIG in the practical situation. A similar analysis procedure can be applied for VPI and PIR regulators without the resonant frequency bandwidth ω_c.

The transfer function of the PIR current regulator in the continuous time domain can be found in Hu *et al.* (2011):

$$C_{\mathrm{PIR}}(s)=K_{\mathrm{p}}+\frac{K_{\mathrm{i}}}{s}+\frac{sK_{\mathrm{r}}}{s^2+\omega_{\mathrm{c}}s+(\pm 6\omega_{\mathrm{l}})^2}, \tag{3}$$

where K_p and K_i are proportional and integral parameters responsible for regulating the DC component respectively, K_r is the resonant parameter to regulate the harmonic component, and ω_c is the bandwidth at the resonant frequency.

Similarly, the transfer function of the VPI current regulator in the continuous time domain can be presented according to Nian and Song (2014):

$$C_{\mathrm{VPI}}(s)=K_{\mathrm{p}}+\frac{K_{\mathrm{i}}}{s}+\frac{K_{\mathrm{pr}}s^2+K_{\mathrm{ir}}s}{s^2+\omega_{\mathrm{c}}s+(\pm 6\omega_{\mathrm{l}})^2}, \tag{4}$$

where K_{pr} and K_{ir} are proportional and integral parameters of the VPI resonant part responsible for regulating the harmonic component, respectively.

Note that the PI part is added to the original VPI (Nian and Song, 2014) and the conventional resonant controller to regulate the fundamental frequency component of the rotor current, while the original VPI and conventional resonant regulators would regulate the 300 Hz harmonic component of the rotor current. Therefore, the PIR and VPI regulators would exhibit as Eqs. (3) and (4). Moreover, the introduction of the ω_c term in Eqs. (3) and (4) is to ensure achievement of the DFIG harmonic control target in the practical wind-farm connected grid.

Comparison of Eqs. (3) and (4) shows that these two regulators have the same PI part for regulating the rotor current fundamental DC component. As for the resonant part, these two regulators have the same denominator, in which $\pm 6\omega_1$ is set as the resonant frequency since the 5th and 7th harmonic components rotate at $-6\omega_1$ and $6\omega_1$ respectively in the $(dq)^+$ frame. Considering that the ideal resonant controller has zero bandwidth at the resonant frequency, which would not be applicable in practical situations (Hu and He, 2009; Hu *et al.*, 2009; Nian and Song, 2014), ω_c is set to ensure achievement of the DFIG harmonic control target in practical applications.

However, the resonant parts of these two regulators each have a different numerator. The numerator of the PIR resonant part is a one-order item determined by the parameter K_r, which can be used to adjust the gain obtained at the resonant frequency. The numerator of the VPI resonant part is a two-order item with two parameters K_{pr} and K_{ir}. These two parameters have been reported in Lascu *et al.* (2009) to be capable of implementing pole-zero cancellation to improve the closed-loop current regulation performance and stability by eliminating the plant pole.

Based on Eqs. (3) and (4), the phase-frequency responses of both PIR and VPI regulators at the resonant frequency $6\omega_1$ can be obtained as

$$\begin{aligned} C_{\mathrm{PIR}}(\mathrm{j}6\omega_{\mathrm{l}}) &= K_{\mathrm{p}}+\frac{K_{\mathrm{i}}}{\mathrm{j}6\omega_{\mathrm{l}}}+\frac{\mathrm{j}6\omega_{\mathrm{l}}K_{\mathrm{r}}}{-(6\omega_{\mathrm{l}})^2+\mathrm{j}6\omega_{\mathrm{l}}\omega_{\mathrm{c}}+(6\omega_{\mathrm{l}})^2} \\ &= K_{\mathrm{p}}+\frac{K_{\mathrm{r}}}{\omega_{\mathrm{c}}}-\mathrm{j}\frac{K_{\mathrm{i}}}{6\omega_{\mathrm{l}}}, \end{aligned} \tag{5}$$

$$\begin{aligned} C_{\mathrm{VPI}}(\mathrm{j}6\omega_{\mathrm{l}}) &= K_{\mathrm{p}}+\frac{K_{\mathrm{i}}}{\mathrm{j}6\omega_{\mathrm{l}}}+\frac{-K_{\mathrm{pr}}(6\omega_{\mathrm{l}})^2+\mathrm{j}6\omega_{\mathrm{l}}K_{\mathrm{ir}}}{-(6\omega_{\mathrm{l}})^2+\mathrm{j}6\omega_{\mathrm{l}}\omega_{\mathrm{c}}+(6\omega_{\mathrm{l}})^2} \\ &= K_{\mathrm{p}}+\frac{K_{\mathrm{ir}}}{\omega_{\mathrm{c}}}+\mathrm{j}\left(\frac{6\omega_{\mathrm{l}}K_{\mathrm{pr}}}{\omega_{\mathrm{c}}}-\frac{K_{\mathrm{i}}}{6\omega_{\mathrm{l}}}\right), \end{aligned} \tag{6}$$

$$\angle C_{\mathrm{PIR}}(\mathrm{j}6\omega_{\mathrm{l}})=\arctan\left(\frac{-K_{\mathrm{i}}/(6\omega_{\mathrm{l}})}{K_{\mathrm{p}}+K_{\mathrm{r}}/\omega_{\mathrm{c}}}\right), \tag{7}$$

$$\angle C_{\mathrm{VPI}}(\mathrm{j}6\omega_{\mathrm{l}})=\arctan\left(\frac{K_{\mathrm{pr}}6\omega_{\mathrm{l}}/\omega_{\mathrm{c}}-K_{\mathrm{ir}}/(6\omega_{\mathrm{l}})}{K_{\mathrm{p}}+K_{\mathrm{ir}}/\omega_{\mathrm{c}}}\right). \tag{8}$$

Comparison of Eqs. (7) and (8) shows that these two phase-frequency equations have the same denominator due to the equivalence of K_r and K_{ir}. However, the numerator of Eq. (8) has one more item $K_{pr}6\omega_1/\omega_c$ than the numerator of Eq. (7). Considering that $K_i/(6\omega_1)\approx 0$ (as K_i is typically set to 1, and $6\omega_1$=1885 rad/s), the PIR phase response (Eq. (7)) at the resonant frequency will be close to 0°.

To satisfy the rule of pole-zero cancellation in the VPI regulator (Lascu *et al.*, 2009), K_{ir} should be chosen as

$$K_{ir}=K_{pr}R_r/(\sigma L_r). \tag{9}$$

Therefore, K_p in the denominator of Eqs. (7) and (8) would be small enough to be neglected compared with K_{ir}/ω_c (K_{pr}=0.5 and K_{ir}=78.5, which follow the rule of pole-zero cancellation of $K_{ir}=157K_{pr}$ due to R_r=0.88 Ω, L_r=0.093 H, σ=0.06; ω_c=20 rad/s). Then Eq. (8) can be simplified as

$$\begin{aligned}\angle C_{VPI}(j6\omega_1)&\approx \arctan\left(\frac{K_{pr}6\omega_1/\omega_c}{K_{ir}/\omega_c}\right)\\&=\arctan(K_{pr}6\omega_1/K_{ir}).\end{aligned} \tag{10}$$

Based on Eq. (10), the phase response of VPI at the resonant frequency will be around 80°–90° since the value of $K_{pr}6\omega_1/K_{ir}$=12 is relatively large.

The bode diagram of the transfer function using both regulators plotted in Fig. 2 can be used to validate the above theoretical analysis, in which K_p=1, K_i=1, ω_c=20 rad/s, ω_1=100π rad/s, K_r=1000, K_{pr}=0.5, and K_{ir}=78.5 are selected based on the rule of pole-zero cancellation. Resonant parts of these two regulators show identical high magnitude gain 34 dB at the resonant frequency 300 Hz, and the gain deceases quickly as the frequency deviates from the resonant point. However, the phase-frequency responses of these two resonant regulators are different. For the two-order numerator of the resonant part applied in the VPI regulator, VPI has a 84° leading phase response while PIR a 0° phase response, which is quite helpful in compensating the inherent phase delay introduced by the inductive inertia nature of DFIG. For the situations with other parameters chosen, similar bode diagrams can be drawn, as shown in the following discussion.

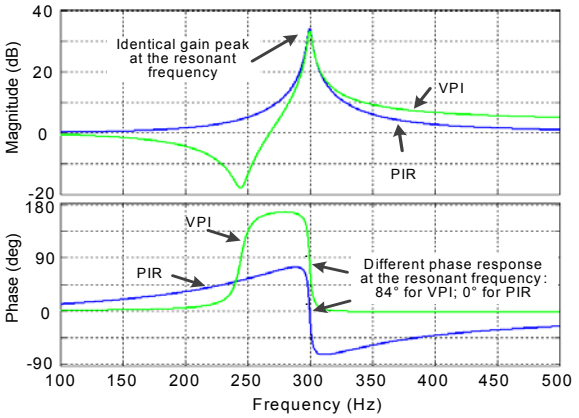

Fig. 2 Bode diagram of PIR and VPI regulators (K_p=1, K_i=1, ω_c=20 rad/s, ω_1=100π rad/s, K_r=1000, K_{pr}=0.5, K_{ir}=78.5)

2.2 Comparison of closed-loop current control of both PIR and VPI resonant parts

To study and compare the harmonic current tracking ability and the stability of resonant parts of these two regulators, closed-loop current control needs to be investigated.

The closed-loop control scheme is as shown in Fig. 3, with the closed-loop transfer function using these two regulators shown as

$$C_{\text{close-PIR}}(s)=\frac{I_{rdq}^*}{I_{rdq}}=\frac{C_{PIR}(s)G_{plant}(s)}{1+C_{PIR}(s)G_{plant}(s)}, \tag{11}$$

$$C_{\text{close-VPI}}(s)=\frac{I_{rdq}^*}{I_{rdq}}=\frac{C_{VPI}(s)G_{plant}(s)}{1+C_{VPI}(s)G_{plant}(s)}, \tag{12}$$

where $C_{PIR}(s)$ and $C_{VPI}(s)$ are as shown in Eqs. (3) and (4), respectively, and $G_{plant}(s)$ is the transfer function of DFIG as shown in Eq. (1).

Note that the electromotive force E_{rdq}^+ in Fig. 3 acts as the decoupling compensation term, which can be regarded as disturbance to the PIR/VPI regulator, calculated as (Hu *et al.*, 2011)

$$\begin{aligned}E_{rdq}^+=&(R_rI_{rdq}^++j\omega_s\sigma L_rI_{rdq}^+)\\&+L_m(U_{sdq}^+-R_sI_{sdq}^+-j\omega_r\psi_{sdq}^+)/L_s,\end{aligned} \tag{13}$$

where R_s and R_r are the stator and rotor resistances respectively, I_{sdq}^+ and I_{rdq}^+ are the stator and rotor current dq-axis components in the $(dq)^+$ synchronous

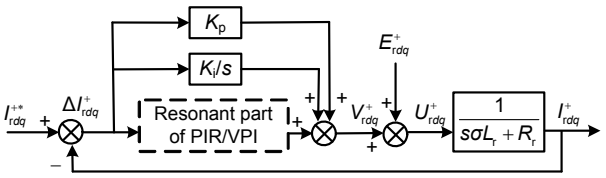

Fig. 3 Schematic of closed-loop current control using PIR/VPI regulators

reference frame respectively, U^+_{sdq} and ψ^+_{sdq} are the stator voltage and flux dq-axis components in the dq+ synchronous reference frame respectively, L_s, L_r, and L_m are the stator, rotor, and mutual inductances respectively, ω_s and ω_r are the slip angular speed and rotor electric angular speed respectively, and $\sigma=1-L_m^2/(L_sL_r)$ is the inductance leakage factor.

Note that the electromotive force E^+_{rdq} terms would be irrelevant to the rotor current 300 Hz AC component regulation. The resonant regulator tuned at 300 Hz would be responsible for restraining the rotor current 300 Hz AC component error and determining the implementation of rotor current harmonic control.

Then, closed-loop transfer function phase response using PIR and VPI at the resonant frequency $6\omega_1$ can be shown as

$$C_{\text{close-PIR}}(\text{j}6\omega_1)=\frac{K_p+K_r/\omega_c-\text{j}K_i/(6\omega_1)}{R_r+K_p+K_r/\omega_c+\text{j}\left(6\omega_1\sigma L_r-K_i/(6\omega_1)\right)}, \quad (14)$$

$$C_{\text{close-VPI}}(\text{j}6\omega_1)=\frac{K_p+K_{ir}/\omega_c+\text{j}\left(K_{pr}\omega_0/\omega_c-K_i/(6\omega_1)\right)}{R_r+K_p+\dfrac{K_{ir}}{\omega_c}+\text{j}\left(6\omega_1\sigma L_r+\dfrac{K_{pr}6\omega_1}{\omega_c}-\dfrac{K_i}{6\omega_1}\right)}. \quad (15)$$

Comparison of Eqs. (14) and (15) shows that Eq. (14) is equal to Eq. (13) if $K_{pr}=0$, which also proves that the major difference between PIR and VPI can be attributed to parameter K_{pr}. The phase-frequency response of Eqs. (14) and (15) can be represented as

$$\angle C_{\text{close-PIR}}(\text{j}6\omega_1)=\arctan\left(\frac{-K_i/(6\omega_1)}{K_p+K_r/\omega_c}\right)-\arctan\left(\frac{6\omega_1\sigma L_r-K_i/(6\omega_1)}{R_r+K_p+K_r/\omega_c}\right), \quad (16)$$

$$\angle C_{\text{close-VPI}}(\text{j}6\omega_1)=\arctan\left(\frac{K_{pr}6\omega_1/\omega_c-K_i/(6\omega_1)}{K_p+K_{ir}/\omega_c}\right)-\arctan\left(\frac{K_{pr}6\omega_1/\omega_c+6\omega_1\sigma L_r-K_i/(6\omega_1)}{R_r+K_p+K_{ir}/\omega_c}\right). \quad (17)$$

By selecting the same parameters as those in Section 2.1, in which K_p and K_i are typically set to 1, $6\omega_1$=1885 rad/s, K_r=1000, ω_c=20 rad/s, R_r=0.88 Ω, the first item of Eq. (16) is equal to zero, and the second item can be simplified as

$$\angle C_{\text{close-PIR}}(\text{j}6\omega_1)\approx-\arctan\left(\frac{6\omega_1\sigma L_r}{R_r+K_p+K_r/\omega_c}\right). \quad (18)$$

The parameters ω_1, σ, L_r, and R_r are all constant in Eq. (18), and considering that K_p is decided by the current regulation ability of the DC signal and system dynamic performance, only K_r and ω_c can be adjusted to decide the phase-frequency response of PIR at the resonant frequency.

Table 1 shows the closed-loop transfer function phase response using PIR with the following parameters: K_p=1, K_i=1, ω_1=100π rad/s and different K_r (500, 1000, 1500, 2000) and ω_c (5, 10, 15, 20 rad/s). The analytical data in Table 1 shows that the closed-loop phase response using the PIR regulator at the resonant frequency will be closer to 0° as the resonant parameter K_r increases or resonant bandwidth ω_c decreases. For instance, the phase response will be −21.4° in the case of K_r=500 and ω_c=20 rad/s, while −5.90° in the case of K_r=2000 and ω_c=20 rad/s. However, during the process of minimizing the closed-loop transfer function phase response by increasing K_r and decreasing ω_c, the control system stability may be compromised (Fig. 4). As shown in Fig. 4, the phase margin would drop from 27° to 16° when K_r increases from 500 to 2000, which will result in an unacceptable extent from the perspective of system stability. Thus, it can be concluded that proper phase margin around the resonant frequency and 0° closed-loop phase response at the resonant frequency can hardly be achieved simultaneously with the PIR current regulator, which will deteriorate DFIG harmonic current control stability and accuracy.

In comparison, the extra item $K_{pr}6\omega_1/\omega_c$ of the VPI regulator plays a dominant role in Eq. (17), as

Table 1 Phase response of the closed-loop transfer function using PIR with different sets of K_r and ω_c at 300 Hz resonant frequency

ω_c (rad/s)	Phase			
	K_r=500	1000	1500	2000
5	−5.91°	−2.98°	−1.99°	−1.50°
10	−11.50°	−5.91°	−3.97°	−2.98°
15	−16.70°	−8.74°	−5.90°	−4.45°
20	−21.40°	−11.50°	−7.80°	−5.90°

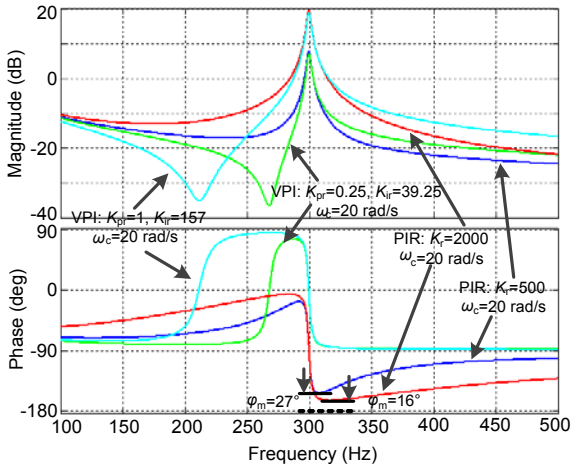

Fig. 4 Bode diagram of open-loop transfer function using both PIR and VPI regulators (K_p=1, K_i=1, ω_c=20 rad/s, ω_1=100π rad/s, K_r=500 or 2000, K_{pr}=0.25 and K_{ir}=39.25 or K_{pr}=1 and K_{ir}=157, R_r=0.88 Ω, σ=0.06, L_r=0.093 H)

$\omega_c << \omega_1$ (ω_c is set at 5, 10, 15, 20 rad/s, and ω_1 is 314 rad/s) and $K_i << 6\omega_1$ ($6\omega_1$ is 1885 rad/s, and K_i is typically set to 1), K_p is typically set at 1, K_{pr} is set at 0.25, 0.5, 0.75, 1, K_{ir}=157K_{pr}, R_r=0.88 Ω, L_r=0.093 H, σ=0.06. Eq. (17) can be simplified as

$$\angle C_{\text{close-VPI}}(\text{j}6\omega_1) \approx \arctan\left(\frac{K_{pr}6\omega_1/\omega_c}{K_p + K_{ir}/\omega_c}\right) - \arctan\left(\frac{K_{pr}6\omega_1/\omega_c + 6\omega_1\sigma L_r}{R_r + K_p + K_{ir}/\omega_c}\right). \quad (19)$$

Based on Eq. (19), considering that $6\omega_1\sigma L_r$ (σ=0.06, L_r=0.093 H) is smaller than $K_{pr}6\omega_1/\omega_c$ (K_{ir}=157K_{pr}=157, following the rule of pole-zero cancellation) and R_r (R_r=0.88 Ω) is quite small, the first and second items of the right-hand side of Eq. (19) will be quite close to each other, which means that in the closed-loop phase-frequency response using the VPI regulator 0° can be achieved at the resonant frequency regardless of the different values of K_{pr}, K_{ir}, and ω_c.

Table 2 shows the closed-loop transfer function phase response using VPI with the following parameters, K_p=1, K_i=1, ω_1=100π rad/s and different sets of K_{pr}, K_{ir}, and ω_c (ω_c is set at 5 rad/s, 10, 15, 20 rad/s and K_{pr} is set at 0.25, 0.5, 0.75, 1, K_{ir}=157K_{pr}). With all the specified parameters, the closed-loop phase response using VPI at the resonant frequency will always be close to 0°, which means that the accurate current tracking can be assured. Fig. 4 also shows that the phase margin will be around 90°, which means that the stable system operation with adequately large phase margin can be achieved. Therefore, stable operation of the closed-loop control system and accurate 0° phase response can be obtained simultaneously, which is quite beneficial for precise closed-loop control of DFIG operation.

Table 2 Phase response of the closed-loop transfer function using VPI with different sets of K_{pr}, K_{ir}, and ω_c at 300 Hz resonant frequency

ω_c (rad/s)	Phase			
	K_{pr}=0.25 K_{ir}=39.25	K_{pr}=0.50 K_{ir}=78.5	K_{pr}=0.75 K_{ir}=117.75	K_{pr}=1 K_{ir}=157
5	−0.062°	−0.014°	−0.006°	−0.003°
10	−0.213°	−0.059°	−0.026°	−0.015°
15	−0.451°	−0.132°	−0.058°	−0.033°
20	−0.728°	−0.222°	−0.101°	−0.058°

Fig. 5 shows the closed-loop bode diagram using both PIR and VPI regulators. The magnitude response of the PIR regulator at 300 Hz is favorably 0 dB, but the phase response is unsatisfactorily −21.4°, which means that the actual rotor current is always 21.4° behind the reference value. Considering that the regulated signal is a harmonic frequency component under $(dq)^+$ that behaves as AC value pulsating at six times fundamental frequency, the phase shift of 21.4° would definitely worsen the tracking precision of the current regulator and increase the tracking error. Furthermore, the PIR regulator would produce an unexpected peak in the vicinity of the resonant frequency in Fig. 5, which means that the noise signal may be possibly amplified within the control closed loop and cause system operation instability as a consequence.

In contrast, when the VPI current regulator is used, the phase response of the closed-loop transfer function at the resonant frequency of 300 Hz is

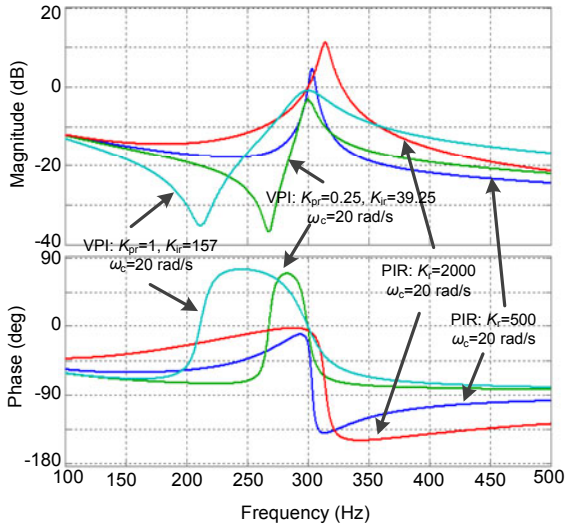

Fig. 5 Bode diagram of closed-loop current control with both PIR and VPI regulators (K_p=1, K_i=1, ω_c=20 rad/s, ω_1=100π rad/s, K_r=500 or 2000, K_{pr}=0.25 and K_{ir}=39.25 or K_{pr}=1 and K_{ir}=157, R_r=0.88 Ω, σ=0.06, L_r=0.093 H)

hopefully 0°. The magnitude response less than 0 dB, however, can be observed when K_{pr} and K_{ir} are chosen to be too small, and can be improved by properly increasing these two parameters. For instance, the gain increases from −3 dB to −1 dB when K_{pr} increases from 0.25 to 1. Thus, the resonant part of VPI is able to achieve not only satisfactory magnitude response but also exact phase response for the actual rotor harmonic current control, and the harmonic control target can be fully accomplished with a zero steady state control error.

Moreover, tiny grid voltage frequency variation and phase lock loop disturbance can hardly be avoided in the practical control system. Thus, the current regulator is required to have strong robustness against tiny grid frequency fluctuation. The maximum phase response change in the VPI regulator in the adjacent area of resonant frequency is 80° and has a relatively smooth phase-frequency changing trend. Thus, tiny grid voltage frequency variation has little negative impact on the control stability of the VPI regulator. However, the maximum phase response change of the PIR regulator will be around 120°, and the changing rate is quite precipitous. In the worst case, when the regulated signal frequency deviates to 308 Hz, the corresponding phase response would be −145°, which would cause serious control error fluctuations in a practical situation.

2.3 Effect of the discretization method on the resonant parts of PIR and VPI

Normally, the current regulator is designed in the continuous time domain and needs to be discretized for use in the digital control system. Several discretization methods are available, including Tustin, zero-order hold, first-order hold, and impulse invariant (Yepes *et al.*, 2010). To maintain the current tracking precision in the practical system, the proposed discretization method should not bring gain attenuation or phase shift to the resonant frequency point.

As reported in Yepes *et al*. (2010), the impulse invariant method can provide an accurate location of the resonant peaks and accurate phase response. The Tustin method is also quite popular when discretizing PI regulators, due to its simple calculation. The discretization results of the resonant parts of PIR and VPI using the impulse invariant and the Tustin method are shown as follows:

$$\begin{aligned}C_{\mathrm{R\_PIR}}^{\mathrm{imp}}(z)=&K_{\mathrm{r}}[z^2-z\mathrm{e}^{-\omega_{\mathrm{c}}T_{\mathrm{s}}/2}\cos(AT_{\mathrm{s}})\\&-\omega_{\mathrm{c}}/(2A)\cdot z\mathrm{e}^{-\omega_{\mathrm{c}}T_{\mathrm{s}}/2}\sin(AT_{\mathrm{s}})]\\&\cdot[z^2-2z\mathrm{e}^{-\omega_{\mathrm{c}}T_{\mathrm{s}}/2}\cos(AT_{\mathrm{s}})+\mathrm{e}^{-\omega_{\mathrm{c}}T_{\mathrm{s}}}]^{-1},\end{aligned}\tag{20a}$$

$$\begin{aligned}C_{\mathrm{R\_PIR}}^{\mathrm{tustin}}(z)=&2K_{\mathrm{r}}T_{\mathrm{s}}(z^2-1)/[(B^2+2D+4)z^2\\&+(2B^2-8)z+(B^2-2D+4)],\end{aligned}\tag{20b}$$

$$\begin{aligned}C_{\mathrm{R\_VPI}}^{\mathrm{imp}}(z)=&K_{\mathrm{pr}}-K_{\mathrm{pr}}(6\omega_1)^2/A\\&\cdot\frac{z\mathrm{e}^{-\omega_{\mathrm{c}}T_{\mathrm{s}}/2}\sin(AT_{\mathrm{s}})}{z^2-2z\mathrm{e}^{-\omega_{\mathrm{c}}T_{\mathrm{s}}/2}\cos(AT_{\mathrm{s}})+\mathrm{e}^{-\omega_{\mathrm{c}}T_{\mathrm{s}}}}+(K_{\mathrm{ir}}-K_{\mathrm{pr}}\omega_{\mathrm{c}})\\&\cdot\frac{z^2-z\mathrm{e}^{-\omega_{\mathrm{c}}T_{\mathrm{s}}/2}\cos(AT_{\mathrm{s}})-\dfrac{\omega_{\mathrm{c}}}{2A}z\mathrm{e}^{-\omega_{\mathrm{c}}T_{\mathrm{s}}/2}\sin(AT_{\mathrm{s}})}{z^2-2z\mathrm{e}^{-\omega_{\mathrm{c}}T_{\mathrm{s}}/2}\cos(AT_{\mathrm{s}})+\mathrm{e}^{-\omega_{\mathrm{c}}T_{\mathrm{s}}}},\end{aligned}\tag{21a}$$

$$\begin{aligned}C_{\mathrm{R\_VPI}}^{\mathrm{tustin}}(z)=&[(4K_{\mathrm{pr}}+2K_{\mathrm{ir}}T_{\mathrm{s}})z^2-8K_{\mathrm{pr}}z\\&+(4K_{\mathrm{pr}}-2K_{\mathrm{ir}}T_{\mathrm{s}})]/[(B^2+2D+4)z^2\\&+(2B^2-8)z+(B^2-2D+4)],\end{aligned}\tag{21b}$$

where $A=\sqrt{(6\omega_1)^2-\omega_{\mathrm{c}}^2/4}$, B=6ω_1T_{s}, D=$\omega_{\mathrm{c}}T_{\mathrm{s}}$.

As shown in Fig. 6a, the discretization result of PIR using the impulse invariant method has almost the same frequency response as the continuous transfer function. When the Tustin method is applied, the results are quite unsatisfactory, with the resonant frequency shifting from 300 Hz to 299.1 Hz, and the

phase response has a delay of −26.1°, which is harmful to regulator stability. A similar conclusion can be made according to the discretization result of the VPI regulator as shown in Fig. 6b.

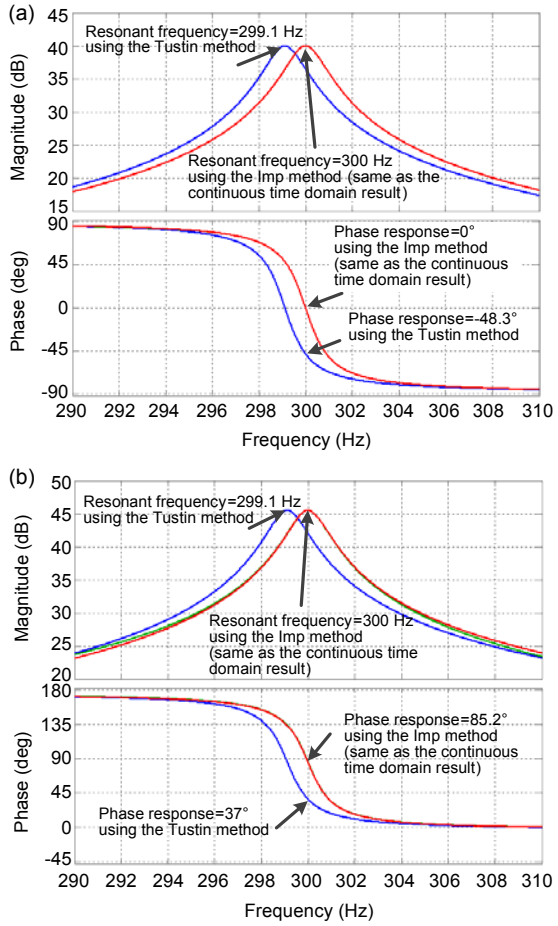

Fig. 6 Discretization results obtained using Tustin and impulse invariant methods with 10 kHz sample frequency

(a) Resonant part of the PIR regulator (ω_c=10 rad/s, ω_1=100π rad/s, K_r=1000); (b) Resonant part of the VPI regulator (ω_c=10 rad/s, ω_1=100π rad/s, K_{pr}=1, K_{ir}=157)

3 Experimental validation

3.1 Experiment setup

The experimental system is developed with a laboratory prototype of a 1 kW DFIG system (Fig. 7), in which the DFIG is driven by a 1.5 kW squirrel cage induction machine which acts as the wind turbine. The induction machine is driven by a general converter. Note that the grid-side converter (GSC) is always adopted to maintain a constant DC-link voltage and thus cannot be helpful in compensating the grid voltage harmonic components or improving the DFIG operation in the harmonic grid (Nian and Song, 2014). Therefore, to better compare the rotor harmonic current tracking capability of PIR and VPI regulators with distorted grid voltage for the rotor-side converter, DC power supply is used in this study to replace the GSC to provide a constant DC-link voltage.

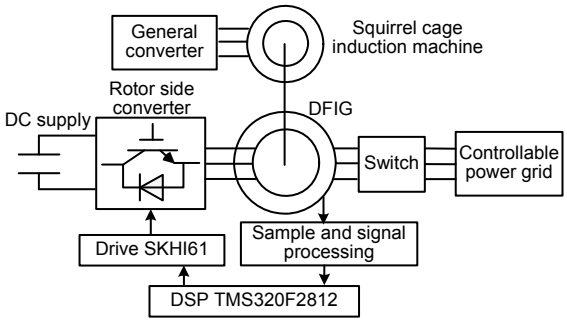

Fig. 7 Block diagram of the experimental system

A controllable three-phase power grid is set up to simulate the practical harmonic power grid (Zeng *et al.*, 2010). During the experiment, grid voltage 5th and 7th order harmonic components are both set at 3%, and the rotor speed is initially set to 800 r/min. Note that the DFIG rotor speed is irrelevant to the PIR/VPI resonant frequency, and therefore the resonant frequency will be set as 300 Hz during the experiment. The whole control strategy is implemented on a TI DSP TMS320F2812, and the driver for IGBT is SEMIKRON SKHI61. The sampling frequency is set to be 10 kHz, and the IGBT switching frequency 5 kHz. The waveforms are acquired by a YOKOGAWA DL750 scope recorder, and the harmonic component analysis is done using a FLUKE NORMA 5000 power analyzer. Parameters of the experimental DFIG are listed in Table 3.

Table 3 Parameters of the experimental DFIG system

Parameter	Value	Parameter	Value
Rated power	1 kW	Mutual inductance, L_m	87.5 mH
Stator voltage	110 V	Stator leakage inductance, $L_{\sigma s}$	5.6 mH
Stator/rotor turns ratio	0.33	Rotor leakage inductance, $L_{\sigma r}$	5.6 mH
Stator resistance, R_s	1.01 Ω	Number of pole pairs	3
Rotor resistance, R_r	0.88 Ω	DC link voltage	200 V

The control diagram of the DFIG system with distorted grid voltage is shown in Fig. 8. First, the grid voltage is decomposed into fundamental and harmonic components, and then the rotor current references are calculated according to the control targets and harmonic voltage components. The rotor current harmonic component references are then transformed to the $(dq)^+$ frame, which will be regulated by the PIR or VPI current regulator. The output voltage of the current regulator is rotated to the rotor oriented frame, and the SVPWM module will be used to produce proper switching signals to the IGBT according to the rotor voltage reference, to implement the operation of the rotor side converter.

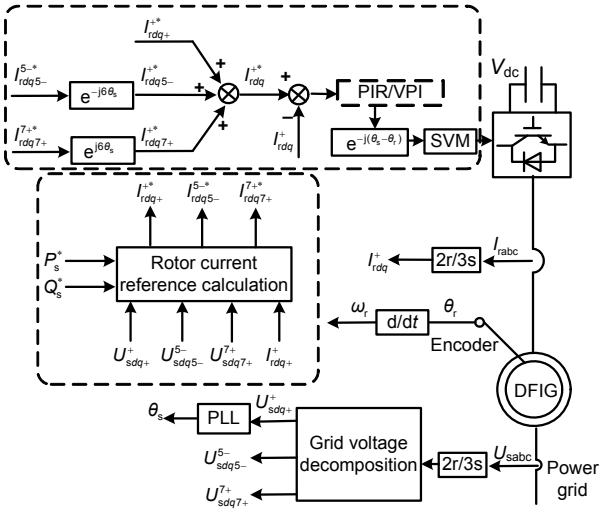

Fig. 8 Control diagram of DFIG with distorted grid voltage using PIR/VPI current regulators

Note that the practical DFIG contains certain inevitable tooth harmonics, which will result in a non-sinusoidal air gap magnetic field and the corresponding stator/rotor current. Such a non-sinusoidal component will always exist during the experiment. Thus, it should be considered as a background harmonic component.

3.2 Experimental results

Fig. 9 shows the DFIG experimental result with non-harmonic grid voltage, and the harmonic analysis data of the stator and rotor current is listed in Table 4. The background harmonic caused by the DFIG itself will result in tiny non-sinusoidal components in both the stator and rotor currents; the 5th and 7th order harmonic components of the stator current are 2.63% and 0.82%, respectively.

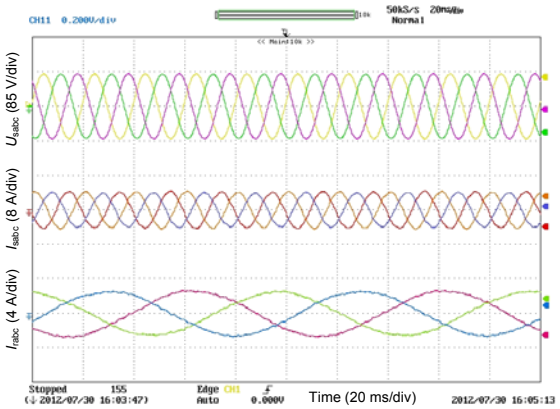

Fig. 9 Experimental results of DFIG stator/rotor currents under the non-harmonic grid voltage condition

Table 4 Harmonic analysis data for different kinds of power grid

Harmonic component	Percentage*			
	Non-harmonic	Distorted#	Distorted, PIR used	Distorted, VPI used
U_s				
5th order	0.83%	2.98%	2.99%	2.97%
7th order	0.38%	2.92%	2.94%	2.95%
I_s				
5th order	2.63%	7.10%	1.92%	1.04%
7th order	0.82%	4.49%	1.23%	0.76%
I_r				
29th order	1.55%	4.48%	0.82%	0.61%
31st order	0.52%	3.11%	0.59%	0.47%

* Ratio of the harmonic component to the respective fundamental component. # Without harmonic control

Fig. 10a shows the experimental results with a distorted grid voltage with 5th and 7th order harmonic components both set at 3.0%. It can be seen that severely distorted stator and rotor currents will occur, which is harmful to the power grid. As the distorted grid voltage contains mainly the 5th and 7th harmonic components, the stator current contains a harmonic component of the same frequency, 250 Hz and 350 Hz. As to the rotor current, considering that the rotor speed is 800 r/min (0.8 p.u., equivalent to 40 Hz), the distorted air gap magnetic field containing a 250 Hz or 350 Hz harmonic component in the stationary frame will generate a 290 Hz (250+40 Hz, due to the negative rotation direction of the 5th harmonic sequence and positive rotor rotation) or 310 Hz

(350−40 Hz, due to the positive rotation direction of the 7th harmonic sequence and positive rotor rotation) harmonic component in the rotor oriented frame. Thus, the 290 Hz and 310 Hz components of the rotor current can be regarded as the 29th and 31st order harmonic components, respectively, given the rotor current basic frequency of 10 Hz. The harmonic analysis results are also available in Table 4. It can be seen that the 5th and 7th order harmonic components of the stator current increase to 7.10% and 4.49%, respectively, due to the existence of grid voltage distortion.

Figs. 10b and 10c give the experimental results of the harmonic control performance of the DFIG stator current with PIR and VPI current regulators, respecttively, and the harmonic analysis results are also listed in Table 4. In contrast to Fig. 10a, stator current harmonic components are greatly restrained with both regulators, and the system has a performance close to that of the non-harmonic power grid shown in Fig. 9. Comparison of the analytical data of the DFIG performance using PIR and VPI regulators shows that the PIR regulator indeed has certain improvements in the stator current harmonic components; i.e., the 5th order stator current decreases from 7.10% to 1.92% and 7th order from 4.49% to 1.23%. However, the PIR regulator fails to regulate the stator current back to ordinary performance in the non-harmonic power grid. When the VPI regulator is adopted, the stator current harmonic components are even smaller than those in the non-harmonic power grid, with the 5th order stator current being 1.04% and the 7th order being 0.76%. Therefore, the VPI regulator will have much better steady state control precision than the PIR regulator.

Table 5 shows the experiment results of DFIG with different discretization methods. Since the Tustin discretization method will cause resonant frequency shift, the rotor current tracking error of using the PIR regulator will result in stator current harmonic 5th sequence of 2.82% and 7th sequence of 2.15%. The impulse invariant method has better performance due to the accurate pole transformation from the continuous domain to the discrete domain. The stator current 5th sequence and 7th sequence can be restrained to 1.92% and 1.23%, respectively. When the VPI regulator is applied, the impulse invariant method still has better performance than the Tustin discretization method, in which the stator current 5th and 7th sequences drop from 1.81% to 1.04% and from 1.27% to 0.76%, respectively.

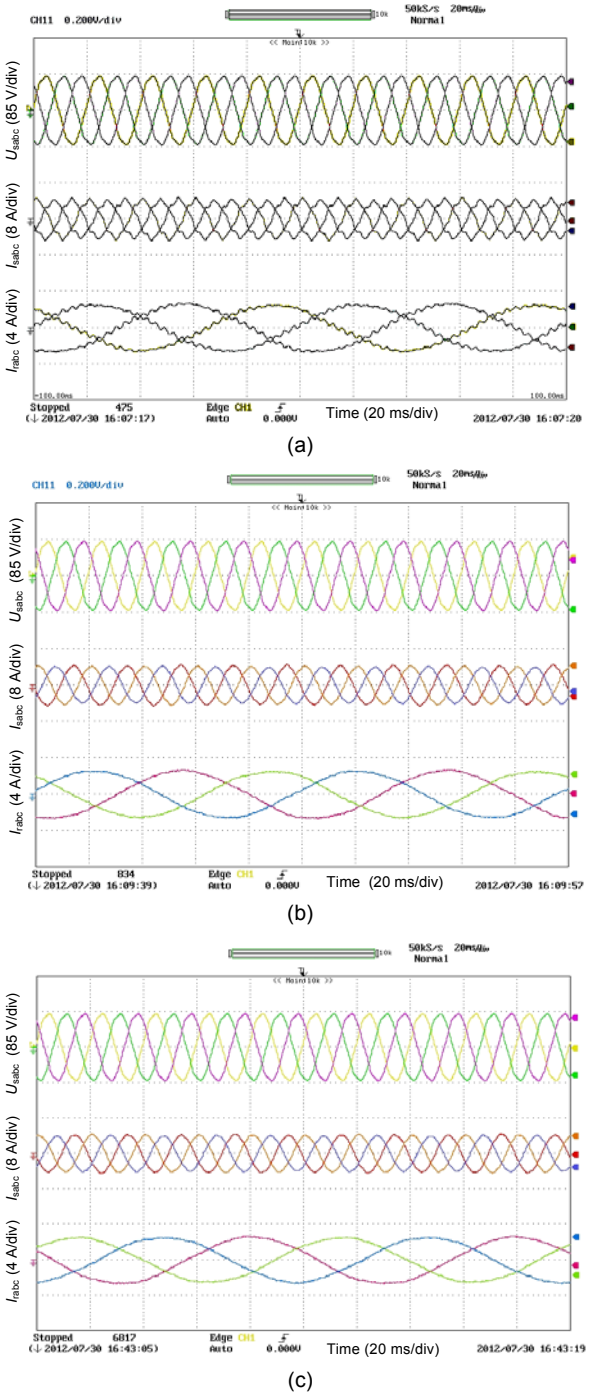

Fig. 10 Experimental results of DFIG stator/rotor currents under a distorted grid voltage condition

(a) Without harmonic control implemented; (b) With the PIR current regulator implemented; (c) With the VPI current regulator implemented

Table 5 Results with different discretization methods*

Harmonic component of I_s	Percentage#			
	Impulse invariant		Tustin	
	PIR	VPI	PIR	VPI
5th order	1.92%	1.04%	2.82%	1.81%
7th order	1.23%	0.76%	2.15%	1.27%

* Experiment conducted with the 5th and 7th order harmonic components of U_s both being 3.0%; 10 kHz sample frequency. # Ratio of the harmonic component to the fundamental component

Fig. 11 shows the experimental results of rotor current transient response during the stator active power reference stepping from 300 W to 600 W using VPI regulators. When active power reference stepping occurs, the VPI regulator is able to adjust the system performance to a steady state within around 40 ms due to operation of the PI part, which is responsible for regulating rotor current DC components. More importantly, no matter whether before or after the active power reference stepping moment, the rotor current control error contains almost a zero 300 Hz pulsation error component, which ensures non-distorted stator current during the transient process.

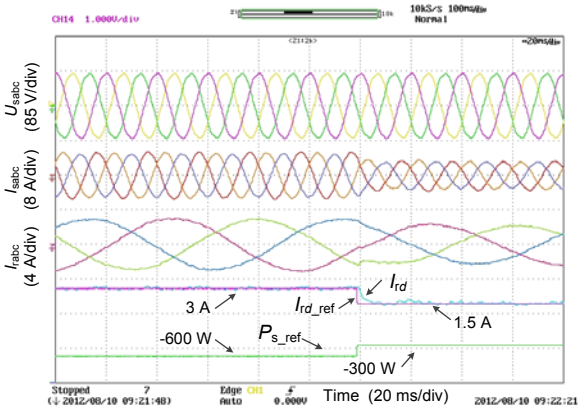

Fig. 11 Experimental results of actual and reference values of rotor currents *d*-axis component under a distorted grid voltage condition with stator output active power reference stepping using the VPI current regulator

Fig. 12 shows the experimental results of DFIG operating from a sub-synchronous state (0.8 p.u.) to a super-synchronous state (1.2 p.u.) when the VPI regulator is applied. During the rotor speed acceleration period, the VPI current regulator can achieve smooth rotor current change, which confirms that the control system can operate normally in both a sub-synchronous state and a super-synchronous state.

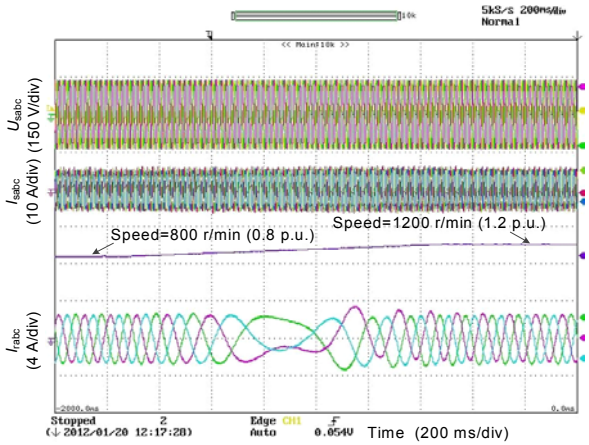

Fig. 12 Experimental results of DFIG stator/rotor currents with the rotor changing from a sub-synchronous state to a super-synchronous state

4 Conclusions

This paper compares the rotor harmonic current tracking capability of the PIR and VPI current regulators for DFIG operation control with distorted grid voltage. The following conclusions can be obtained from theoretical analysis and experimental validation:

1. Aimed at DFIG operation with harmonic grid voltage, the VPI regulator has a much larger phase margin than the PIR regulator, which is beneficial for stable closed-loop operation of DFIG.

2. The VPI regulator exhibits an accurate steady state closed-loop operation with 0 dB magnitude response and 0° phase response, while the PIR regulator fails to achieve 0° phase response at the resonant frequency.

References

Arbi, J., Ghorbal, M.J.B., Slama-Belkhodja, I., Charaabi, L., 2009. Direct virtual torque control for doubly fed induction generator grid connection. *IEEE Trans. Ind. Electron.*, **56**(10):4163-4173. [doi:10.1109/TIE.2009.2021590]

Bojoi, R.I., Griva, G., Bostan, V., Guerriero, M., Farina, F., Profumo, F., 2005. Current control strategy for power conditioners using sinusoidal signal integrators in synchronous reference frame. *IEEE Trans. Power Electron.*, **20**(6):1402-1412. [doi:10.1109/TPEL.2005.857558]

Etxeberria-Otadui, I., de Heredia, A.L., Gaztañaga, H., Bacha, S., Raúl Reyero, M.R., 2006. A single synchronous frame hybrid (SSFH) multifrequency controller for power active filters. *IEEE Trans. Ind. Electron.*, **53**(5):1640-1648. [doi:10.1109/TIE.2006.881994]

Fukuda, S., Imamura, R., 2005. Application of a sinusoidal internal model to current control of three-phase utility-interface converters. *IEEE Trans. Ind. Electron.*, **52**(2): 420-426. [doi:10.1109/TIE.2005.843914]

Gambica, 2005. Managing Harmonics—a Guide to ENA Engineering Recommendation G5/4 – 1. The Gambica Association Limited, London.

Hu, J.B., He, Y.K., 2009. Reinforced control and operation of DFIG-based wind-power-generation system under unbalanced grid voltage conditions. *IEEE Trans. Energy Conv.*, **24**(4):905-915. [doi:10.1109/TEC.2008.2001434]

Hu, J.B., He, Y.K., Xu, L., Williams, B.W., 2009. Improved control of DFIG systems during network unbalance using PI–R current regulators. *IEEE Trans. Ind. Electron.*, **56**(2):439-451. [doi:10.1109/TIE.2008.2006952]

Hu, J.B., He, Y.K., Xu, L., 2010. Improved rotor current control of wind turbine driven doubly-fed induction generators during network voltage unbalance. *Electr. Power Syst. Res.*, **80**(7):847-856. [doi:10.1016/j.epsr.2009.12.010]

Hu, J.B., Nian, H., Xu, H.H., He, Y.K., 2011. Dynamic modeling and improved control of DFIG under distorted grid voltage conditions. *IEEE Trans. Energy Conv.*, **26**(1): 163-175. [doi:10.1109/TEC.2010.2071875]

IEEE Standard 519-1992. IEEE Recommended Practices and Requirements for Harmonic Control in Electrical Power Systems. IEEE, New York. [doi:10.1109/IEEESTD.1993.114370]

Iwanski, G., Koczara, W., 2008. DFIG-based power generation system with UPS function for variable-speed applications. *IEEE Trans. Ind. Electron.*, **55**(8):3047-3054. [doi:10.1109/TIE.2008.918473]

Lascu, C., Asiminoaei, L., Boldea, I., Blaabjerg, F., 2007. High performance current controller for selective harmonic compensation in active power filters. *IEEE Trans. Power Electron.*, **22**(5):1826-1835. [doi:10.1109/TPEL.2007.904060]

Lascu, C., Asiminoaei, L., Boldea, I., Blaabjerg, F., 2009. Frequency response analysis of current controllers for selective harmonic compensation in active power filters. *IEEE Trans. Ind. Electron.*, **56**(2):337-347. [doi:10.1109/TIE.2008.2006953]

Li, Z.X., Li, Y.H., Wang, P., Zhu, H.B., Liu, C.W., Gao, F.Q., 2010. Single-loop digital control of high-power 400-Hz ground power unit for airplanes. *IEEE Trans. Ind. Electron.*, **57**(2):532-543. [doi:10.1109/TIE.2009.2033490]

Liu, C.J., Blaabjerg, F., Chen, W.J., Xu, D.H., 2012. Stator current harmonic control with resonant controller for doubly fed induction generator. *IEEE Trans. Power Electron.*, **27**(7):3207-3220. [doi:10.1109/TPEL.2011.2179561]

Liu, C.J., Xu, D.H., Zhu, N., Blaabjerg, F., Chen, M., 2013. DC-voltage fluctuation elimination through a DC-capacitor current control for DFIG converters under unbalanced grid voltage conditions. *IEEE Trans. Power Electron.*, **28**(7):3206-3218. [doi:10.1109/TPEL.2012.2223829]

Luna, A., Lima, F.K.A., Santos, D., Rodríguez, P., Watanabe, E.H., Arnaltes, S., 2011. Simplified modeling of a DFIG for transient studies in wind power applications. *IEEE Trans. Ind. Electron.*, **58**(1):9-20. [doi:10.1109/TIE.2010.2044131]

Muller, S., Deicke, M., de Doncker, R.W., 2002. Doubly fed induction generator systems for wind turbines. *IEEE Ind. Appl. Mag.*, **8**(3):26-33. [doi:10.1109/2943.999610]

Nian, H., Song, Y.P., 2014. Direct power control of doubly fed induction generator under distorted grid voltage. *IEEE Trans. Power Electron.*, **29**(2):894-905. [doi:10.1109/TPEL.2013.2258943]

Pena, R., Cardenas, R., Reyes, E., Clare, J., Wheeler, P., 2011. Control of a doubly fed induction generator via an indirect matrix converter with changing DC voltage. *IEEE Trans. Ind. Electron.*, **58**(10):4664-4674. [doi:10.1109/TIE.2011.2109334]

Ramos, C.J., Martins, A.P., Carvalho, A.S., 2007. Rotor Current Controller with Voltage Harmonics Compensation for a DFIG Operating under Unbalanced and Distorted Stator Voltage. 33rd Annual Conf. of the IEEE Industrial Electronics Society, p.1287-1292. [doi:10.1109/IECON.2007.4459938]

Singh, G.K., 2009. Power system harmonics research: a survey. *Eur. Trans. Electr. Power*, **19**(2):151-172. [doi:10.1002/etep.201]

Xu, L., Wang, Y., 2007. Dynamic modeling and control of DFIG based wind turbines under unbalanced network conditions. *IEEE Trans. Power Syst.*, **22**(1):314-323. [doi:10.1109/TPWRS.2006.889113]

Xu, L., Zhi, D.W., Williams, B.W., 2009. Predictive current control of doubly fed induction generators. *IEEE Trans. Ind. Electron.*, **56**(10):4143-4153. [doi:10.1109/TIE.2009.2017552]

Yepes, A.G., Freijedo, F.D., Doval-Gandoy, J., López, O., Malvar, J., Fernandez-Comesaña, P., 2010. Effects of discretization methods on the performance of resonant controllers. *IEEE Trans. Power Electron.*, **25**(7):1692-1712. [doi:10.1109/TPEL.2010.2041256]

Yuan, X.M., Merk, W., Stemmler, H., Allmeling, J., 2002. Stationary-frame generalized integrators for current control of active power filters with zero steady-state error for current harmonics of concern under unbalanced and distorted operating conditions. *IEEE Trans. Ind. Appl.*, **38**(2): 523-532. [doi:10.1109/28.993175]

Zeng, R., Nian, H., Zhou, P., 2010. A Three-Phase Programmable Voltage Sag Generator for Low Voltage Ride-Through Capability Test of Wind Turbine. IEEE Energy Conversion Congress and Exposition, p.305-311. [doi:10.1109/ECCE.2010.5618020]

Zmood, D.N., Holmes, D.G., 2003. Stationary frame current regulation of PWM inverters with zero steady-state error. *IEEE Trans. Power Electron.*, **18**(3):814-822. [doi:10.1109/TPEL.2003.810852]